JOURNAL OF SOLID STATE CHEMISTRY 102, 54–68 (1993)

Molybdenum Cluster Chalcogenides: *In Situ* X-Ray Studies on the Formation of $Cu_xMo_6S_8$ via Electron/Ion Transfer

C. FISCHER,* E. GOCKE, U. STEGE, AND R. SCHÖLLHORN†

Technische Universität Berlin, Institut für Anorganische und Analytische Chemie, Strasse des 17. Juni 135, D-1000 Berlin 12, Germany

Received January 7, 1992; in revised form May 15, 1992; accepted May 18, 1992

Systematic structural investigations have been performed on the formation of the ternary Chevrel phase system $Cu_xMo_6S_8$ by topotactic intercalation of copper into Mo_6S_8 via electron/ion transfer reactions. In high-temperature synthesis the homogeneity range of $Cu_xMo_6S_8$ formation corresponds to $1.8 \leq x \leq 3.66$, while by galvanostatic or potentiostatic reduction of binary Mo_6S_8 at ambient temperature in aqueous $CuSO_4$ or aprotic $CuCl/CH_3CN$ electrolyte the terminal rhombohedral phase $Cu_4Mo_6S_8$ with the maximum number of electrons per Mo_6 cluster can be obtained. The phase range $1 \leq x \leq 4$ of $Cu_xMo_6S_8$ as obtained by galvanostatic reduction of Mo_6S_8 in aqueous $CuSO_4$ electrolyte has been determined by *in situ* X-ray experiments. Warburg oxygen manometry has proved to be a new and powerful analytical tool for examination of the Cu content of ternary phase $Cu_xMo_6S_8$. Thermodiffractometry and ^{63}Cu NMR studies of $Cu_2Mo_6S_8$ (high-temperature phase) reveal a phase-transition rhombohedral/triclinic in a broad temperature range between 285 and 200 K. Superconducting properties (temperature-dependent ac susceptibility) of high temperature and electrochemically prepared Cu phases are reported.

Introduction

The binary and ternary molybdenum cluster chalcogenides (Chevrel phases) with the compositions Mo_6X_8 and $A_xMo_6X_8$ (X = S, Se; A = main-group or transition metal) are known to exhibit unusual physical properties—in particular with respect to superconducting behavior—which depend strongly upon the nature of the chalcogen anion X, the nature of the ternary metal A, and the stoichiometry of the latter (*1*, *2*). The structure of the binary phases can be described by a three-dimensional arrangement of Mo_6X_8 units, which themselves consist of X_8 cubes surrounding the distorted Mo_6 octahedra (Fig. 1). This framework system leads to intersecting "channels" of vacant lattice sites along the three rhombohedral axes, which are partially occupied in the case of the ternary phases by the metal atoms A (Fig. 2). Moreover, it has been shown recently that the Mo_6X_8 cluster phases exhibit remarkable properties in terms of chemical reactivity. They are able to undergo reversible topotactic redox reactions at ambient temperature via electron/ion transfer according to the equation (*3*, *4*).

$$xA^+ + xe^- + \square_n[Mo_6X_8] \rightleftarrows (A^+)_x\square_{n-x}[Mo_6X_8]^{x-}, \quad (1)$$

where $\square$ = vacant lattice site.

* Present address: Hahn-Meitner-Institut Berlin, Bereich S, Glienicker Strasse 100, D-1000 Berlin 39, Germany.

† To whom correspondence should be addressed.

0022-4596/93 $5.00

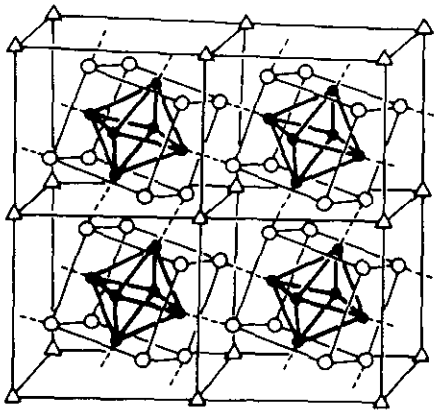

FIG. 1. Structure of binary molybdenum cluster chalcogenides Mo_6X_8 (X = S, Se, Te): ●, Mo; ○, X; Δ, vacant "channel" positions at the unit cell origin.

The electrons are accepted by the lowest lying vacant energy level of the host band (conduction band), which acts as an electron sink, and the matrix becomes a macroanion $[Mo_6X_8]^{x-}$. The negative excess charge is compensated by the simultaneous uptake of mobile cations A^+, which occupy empty sites in the lattice channels. Reaction (1) describes the conversion of an electronic conductor to an electronic/ionic conductor by an intercalation process, which can be performed either by chemical reaction or by electrochemical techniques in appropriate electrolytes (5). The reaction described allows the reversible modification of the physical properties of the Mo_6X_8 matrix via chemical reactions at ambient temperature and it is an interesting alternative route for preparing new materials that makes use of the consequences of kinetics in low-temperature synthesis, which exploits the fact that metastable states can be stabilized at lower temperatures.

One aspect of particular interest with respect to the chemical reactivity of these systems is the upper stoichiometry limit x_{max} of the guest cations. The latter can be treated in a simple model in terms of a competition between geometrical and electronic restraints (4, 6). For small ions the structure provides 12 potential formal lattice sites around the unit cell origin with distorted tetrahedral symmetry (1, 2). The first ring has six positions [Cu(1)] close to the unit cell origin, forming the "inner" sites; a second ring with six positions [Cu(2)] which form the "outer" sites is located around the inner positions (Fig. 2b). In electronic terms

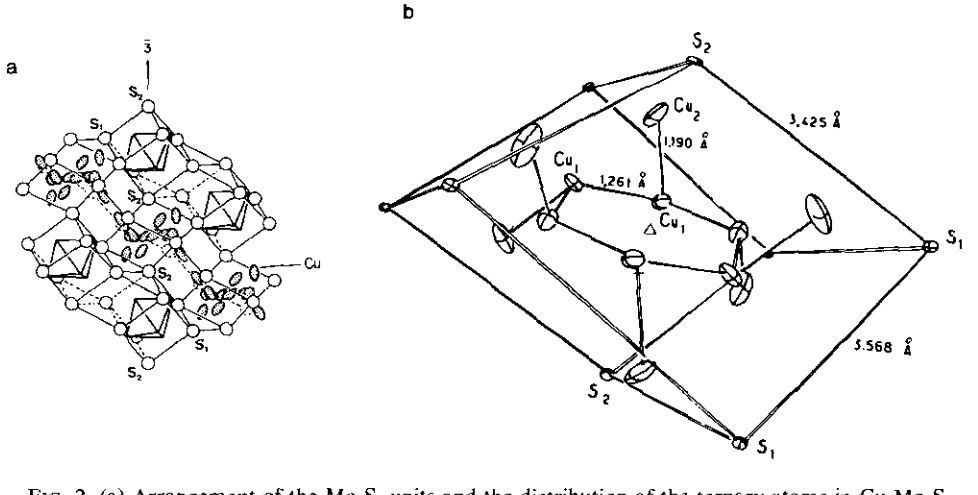

FIG. 2. (a) Arrangement of the Mo_6S_8 units and the distribution of the ternary atoms in $Cu_xMo_6S_8$. (b) A perspective view of the six inner Cu(I) and outer Cu(II) positions in $Cu_{1.8}Mo_6S_8$. Δ, unit cell origin; the threefold axis goes through S2–Δ–S2 (adapted from Ref. (1)).

the maximum charge transfer predicted is equivalent to $4e^-/Mo_6S_8$, resulting in the maximal insertion of, e.g., four monovalent cations A^+ or two bivalent cations A^{2+}. This is a consequence of the ionic model discussed by Yvon (*1*), which considers the electron-deficient Mo_6 cluster in Mo_6S_8 (number of electrons per cluster (NEC) = 20) that can formally take up four additional electrons in order to establish 12 two-electron Mo–Mo bonds (NEC = 24).

Chevrel *et al.* were the first to report on nonstoichiometric $Cu_xMo_6S_8$ compounds (*7, 8*). Studies of low-temperature relationships in terms of structural phase transitions and superconducting properties soon followed (*9*). The system Cu/Mo_6S_8 is currently the only ternary molybdenum cluster chalcogenide system for which the phase diagram has been extensively studied (*10, 11*). The homogeneity range of the $Cu_xMo_6S_8$ phase prepared by high-temperature synthesis extends from $x = 1.2$ to $x < 4$. The limits of the rhombohedral phase are strongly temperature dependent, so that the range $1.2 \leq x < 1.8$ is metastable at room temperature and can be retained only by quenching. The first investigations on the intercalation of Cu into Mo_6S_8 at ambient temperature were performed by electrochemical techniques (*12, 13*). Galvanostatic titration of the binary molybdenum cluster sulfide in aqueous Cu electrolyte led to the identification of rhombohedral $Cu_xMo_6S_8$ with $1.2 \leq x \leq 3.2$. $Cu_2Mo_6S_8$ was found to exhibit the highest superconducting transition temperature (T_c = 10.8 K) over the mentioned homogeneity range (*13*). An upper limit of $x = 5$ was reported subsequently by coulometric titration of the host lattice via Cu-containing solid electrolyte at 400 K (*14*). Measurements of the chemical diffusion coefficient $\tilde{D}$ using a solid state electrolyte yielded values of 10^{-7} to 10^{-5} $cm^2 \cdot sec^{-1}$ for $Cu_{1.5}Mo_6S_8$ and $Cu_{3.37}Mo_6S_8$ at 440 K (*15*).

Since the Cu system is of particular importance for an understanding of charge transfer with regard to the upper stoichiometry limit x_{max} of the guest cations, we have undertaken a thorough study of structural and compositional changes with Mo_6S_8 as the host lattice. These investigations have been supplemented by extensive *in situ* X-ray studies to establish the phase regions of the intercalation compounds.

Experimental

The binary host lattice Mo_6S_8 was prepared from the ternary compound $Cu_2Mo_6S_8$. The latter was obtained by heating the elements (stoichiometric ratio, purity >99.9%) in sealed quartz ampoules for 24 hr to 450°C and thereafter for 24 hr to 700°C. After each heating period, the loose powder in the ampoules was agitated to achieve homogeneous products. The final heating mode was 1100°C for 24 hr with subsequent slow cooling over 10 days. Ternary molybdenum cluster sulfides with other nominal copper contents were prepared in the same way. Treatment of the copper compounds with aqueous $FeCl_3$/0.1 *N* HCl solution (leaching technique) led to the quantitative removal of Cu with the formation of Mo_6S_8 (lattice parameters given in Table I). Anodic oxidation of the ternary phases in 0.1 *N* H_2SO_4 led also to a quantitative copper deintercalation. EDAX studies confirmed the absence of copper ions in both cases. Analytical data were obtained by wet analysis, atomic absorption spectrometry, and microanalysis. The values found for the binary phase were as follows: *Anal.* Found (calcd) for Mo_6S_8: Mo, 69.04 (69.18); S, 30.88 (30.82).

X-ray powder measurements were made with the Simon–Guinier technique from samples sealed in lithium borate glass capillaries. Due to the sensitivity of the intercalated phases to oxygen and water, all operations had to be carried out in closed systems under an argon atmosphere. Mo_6S_8 was similarly stored under an inert gas atmosphere,

TABLE I

RHOMBOHEDRAL AND HEXAGONAL LATTICE PARAMETERS OF Mo_6S_8 AND $Cu_xMo_6S_8$

x	a_R (pm)	α_R (°)	a_H (pm)	c_H (pm)	c (a)	$V_H \cdot 10^6$ (pm^3)
0	642.40(3)	91.26(1)	918.4(2)	1088.0(3)	1.1844	794.63
1.00	647.85(3)	94.17(1)	949.8(1)	1037.4(2)	1.0923	810.48
1.25	648.57(4)	94.36(2)	951.9(2)	1034.1(2)	1.0863	811.44
1.50	649.32(3)	94.57(1)	954.4(3)	1031.1(4)	1.0804	813.28
1.88	650.37(3)	94.91(2)	959.8(3)	1025.8(3)	1.0688	818.29
2.10	651.43(3)	95.14(3)	967.3(2)	1020.4(2)	1.0549	826.77
2.30	652.50(3)	95.22(2)	969.3(2)	1021.0(3)	1.0533	830.81
2.56	654.21(4)	95.32(3)	972.4(2)	1022.7(3)	1.0518	837.44
2.97	657.64(4)	95.58(1)	974.0(3)	1022.3(3)	1.0497	839.82
3.20	658.79(3)	95.60(3)	975.4(3)	1023.6(3)	1.0494	843.34
3.60	660.33(4)	95.62(2)	978.1(3)	1025.8(4)	1.0487	849.87
4.00	661.63(3)	95.66(2)	979.7(3)	1026.9(3)	1.0481	853.64

Note. Data were obtained from galvanostatic reduction of Mo_6S_8 in aqueous $CuSO_4$ electrolyte at 300 K.

since we found that on exposure to air slow oxidation (catalyzed by Mo) proceeds under formation of molybdenum oxide hydrates and sulfuric acid. Additional diffraction patterns and structural phase transitions at low temperatures were obtained with a powder diffractometer (Siemens D 500, Cu $K\alpha$ radiation) equipped with a position-sensitive detector which allows rapid data collection.

Electrochemical reactions were performed at 300 K in three electrode galvanic cells with commercial and homemade equipment to monitor the current and potential. Galvanostatic titration, potentiostatic reaction with integration of the charge consumed, oxidation/reduction cycling, short circuit runs, and EMF measurements (equilibrium potentials) were used for the electrochemical study of the reactions. The working electrodes consisted of pressed polycrystalline samples with 1% wt Teflon as a binder. Cu plates served as counterelectrodes; the potentials of the coulometric titration of the host lattice were measured vs Cu^0 (small rods). Dry, clean Cu^ICl of analytical purity in high-purity acetonitrile (residual water content 20 ppm as determined by Karl–Fischer titration) served as the aprotic electrolyte. Reactions with Cu^{2+} were performed in aqueous electrolyte (saturated $CuSO_4$ solution). All operations were carried out in an inert gas atmosphere. For evaluation of the chemical diffusion coefficient $\tilde{D}$ the galvanostatic intermittent titration technique (GITT) was used (*16*).

A specially constructed plexiglass galvanic cell was used to perform *in situ* X-ray studies during the coulometric titration of the host lattice (Fig. 3). An X-ray transparent adhesive tape (Tesa Spezial) was used as the window in the diffraction plane. The

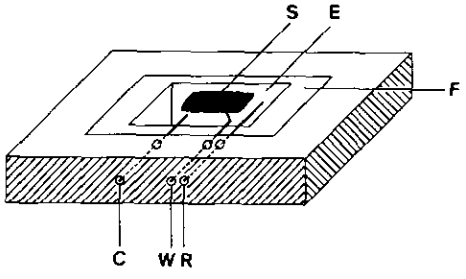

FIG. 3. Plexiglass electrochemical cell for *in situ* X-ray studies: S, sample; E, electrolyte; F, X-ray transparent film; W, C, R, working, counter, and reference electrodes.

working electrode for this cell arrangement consisted of a thin pellet of Mo_6S_8 mixed with 1% wt Teflon binder (surface, 1 cm^2; weight, approximately 50 mg; thickness, 0.1 mm). After adjustment of the working electrode in the diffraction plane of the electrochemical cell, it was contacted with platinum cement. The counterelectrode consisted of Cu wire; a small Cu rod was used as the reference electrode.

For control purposes the copper content of the intercalation compounds was routinely checked by electrogravimetry after decomposition of the Cu phases in dilute HCl solution. The integral Cu content of ternary phases $Cu_xMo_6S_8$ was determined by Warburg oxygen manometry. Upon dissolution of $(Cu^+)_x[Mo_6X_8]^{x-}$ in aqueous acid solutions in a closed system, Cu^I will be oxidized to Cu^{II}, resulting in consumption of oxygen, according to Eq. (2), which can be detected in the closed system of the Warburg apparatus:

$$(Cu^+)_x[Mo_6S_8]^{x-} + x/4O_2 + xH^+ \rightarrow Mo_6S_8 + xCu^{2+} + x/2H_2O. \quad (2)$$

Critical temperatures T_c for the transition normal conductivity/superconductivity have been measured by the ac susceptibility technique (Meissner effect). ^{63}Cu NMR measurements were performed at 79.515 MHz on a Bruker CXP 300 FT spectrometer. As an external reference for the determination of the chemical shift, solid Cu^ICl was used. Further details and results of the temperature-dependent NMR studies will be published elsewhere (*17*).

Results and Discussion

Formation of $Cu_xMo_6S_8$ by Galvanostatic Cathodic Reduction of Mo_6S_8 in Aqueous Cu^{2+} Electrolyte

The potential/charge transfer diagram for the electrochemical intercalation of Cu^{2+} into the host lattice by cathodic reduction in the galvanic cell $Cu^0//Cu^{2+}$, $H_2O//Mo_6S_8$ is given in Fig. 4a. Figure 4b illustrates the corresponding changes in the hexagonal lattice parameters observed during the reaction with increasing integral Cu content x of the reaction products, as determined analytically. Since the oxidation state of copper in the ternary transition metal chalcogenides is Cu^{1+} (*18*), two electrons are required for the intercalation of one Cu ion from aqueous $Cu^{II}SO_4$ solution (Eq. (3)): at the phase boundary of solid//electrolyte Cu^{2+} will be reduced to Cu^{1+}; during the electron/ion-transfer process an additional electron will be taken up into the upper band level of the molybdenum cluster sulfide, while the guest ions Cu^{1+} fill the vacant lattice sites. The integral analytical Cu content $x(Cu/Mo_6S_8)$—determined by electrogravimetry and Warburg manometry—of samples collected at given values of the electrochemical charge transfer $n(e^-/Mo_6S_8)$ corresponds linearly with n according to $x = n/2$; i.e., no side reactions occur:

$$xCu^{2+} + 2xe^- + Mo_6S_8 \rightleftarrows (Cu^+)_x[Mo_6S_8]^{x-}. \quad (3)$$

The critical values for the intercalation of guest ions into the Mo_6S_8 host lattice must be $\leq \sim 126$ pm, since rare earth ions with hard-sphere radii of ~100–110 pm cannot be intercalated into the binary phase or deintercalated from ternary compounds prepared by thermal reaction, while Ag^+ ions can still be inserted. We observed a strong influence however of kinetics upon the reaction Cu/Mo_6S_8, indicated by a noticeable variation in apparent potential with the current density. This is obviously due to the limited mobility of the copper ion ($r_{Cu^+} = 96$ pm) in the Mo_6S_8 framework. It turned out that under the conditions used, the optimal current density for the intercalation process is given by value of 0.2 mA · cm^{-2}.

Analytical data reveal that the linearity of $x = n/2$ no longer applies for significantly lower current densities, where the increase

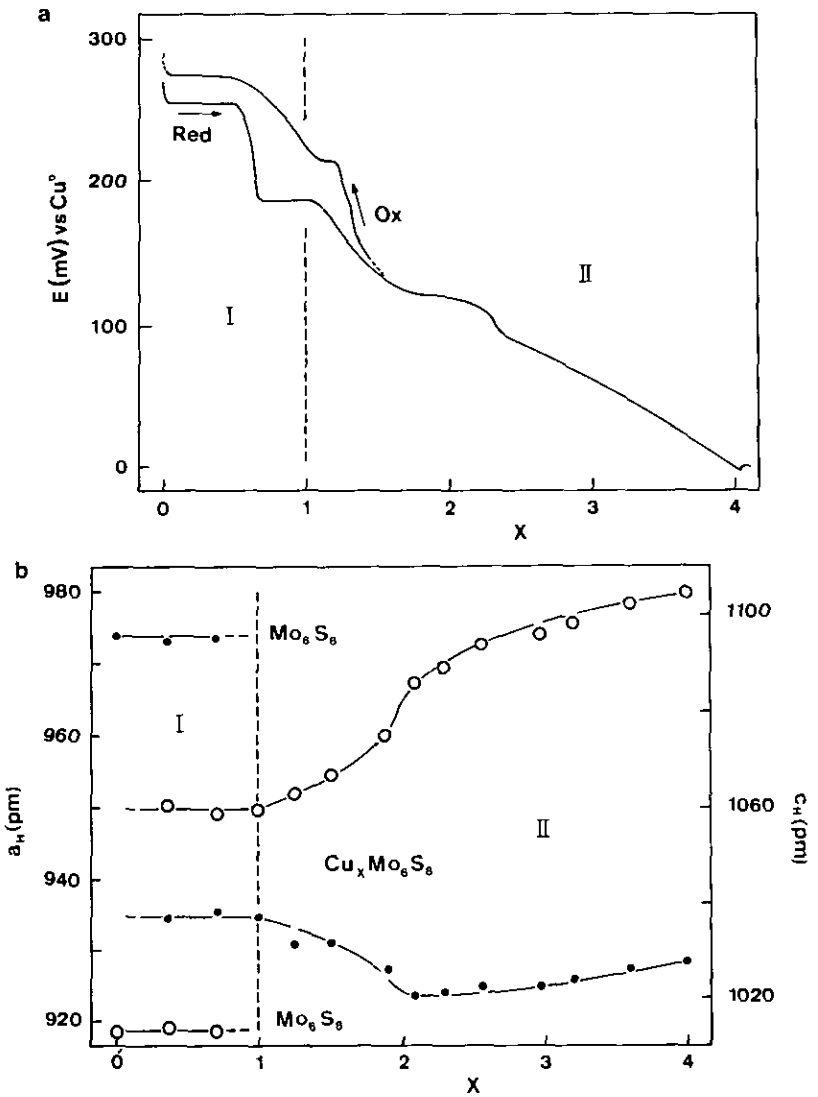

FIG. 4. Formation of $Cu_xMo_6S_8$ by galvanostatic cathodic reduction of Mo_6S_8 electrodes in aqueous $CuSO_4$ electrolyte at 300 K: (a) Change in potential E (vs Cu^0) of the working electrode with the integral Cu content x; (b) change in hexagonal lattice parameters (a_H = ○, c_H = ●) with x.

in Cu content is smaller than the value calculated. At low current densities a portion of the Cu^{2+} ions is reduced on the electrode surface and diffuses back into the aqueous solution under disproportionation or is deposited as Cu_2O; the overall electrochemical charge transfer values thus become formally larger before the potential of Cu deposition is reached. On the other hand, higher current densities lead for kinetic reasons to premature reaching of the potential of Cu deposition before the terminal phase with maximum Cu content is obtained. Figure 4a presents the potential/charge transfer dia-

grams obtained on galvanostatic cathodic reduction and anodic reoxidation of Mo_6S_8 and $Cu_xMo_6S_8$, respectively, in a saturated aqueous $CuSO_4$ solution at 300 K. In terms of thermodynamics the potential plateaus appearing in the cathodic current seem to represent two separate two-phase systems with $0 \leq x \leq 0.5$ and $0.66 \leq x \leq 1.1$, since the potentials remain constant (i.e., ΔG = const.). With further reduction the continuous change in potential should correspond to a nonstoichiometric phase region. The end point of the coulometric titration of the host lattice is attained after a transfer of $8e^-/Mo_6S_8$, i.e., $4Cu/Mo_6S_8$, where the electrode potential becomes identical with the potential of the copper reference electrode and metal deposition occurs. The maximum charge transfer observed is thus in formal agreement with the predictions from the ionic/covalent structure model (*1*) and the band structure calculations (*6, 19*) for the molybdenum cluster sulfide. The terminal phase $Cu_4Mo_6S_8$ is a new metastable compound which is accessible only by isothermal topotactic reaction at low temperature.

The electrochemical intercalation of copper ions into the binary molybdenum cluster sulfide is completely reversible, as determined analytically. On anodic oxidation of the terminal phase, the same sequence of reactions is found in the reverse direction up to a deintercalation stage of $2.5Cu/Cu_4Mo_6S_8$. At copper contents lower than $Cu_{1.5}Mo_6S_8$, however, deviations are observed. As illustrated in Fig. 4a the range from $x = 0.5$ to $x = 1.5$ in $Cu_xMo_6S_8$ is characterized by a significant hysteresis of the potentials for forward and back reaction. The final product after a charge transfer of $8e^-/Cu_4Mo_6S_8$ is the binary phase Mo_6S_8 with lattice parameters identical to those given in Table I.

The structural changes in ternary copper phases $Cu_xMo_6S_8$ during the intercalation process were investigated by *in situ* X-ray studies. Figure 4b shows the hexagonal lattice parameters of the intercalation system $Cu_xMo_6S_8$ at selected values of the integral copper content x. Table I presents the lattice parameters and unit cell volumes of the starting phase and of ternary Cu compounds. X-ray diffraction data for region I ($0 < x < 1$) clearly show the coexistence of two phases: Mo_6S_8 and $Cu_1Mo_6S_8$ (Eq. (4)). Selected X-ray diffraction patterns recorded *in situ* are given in Fig. 5a. In Fig. 6 the changes in the relative intensities of the two coexisting phases Mo_6S_8 and $Cu_1Mo_6S_8$ are given as a function of the integral copper content:

$$\text{Two-phase region: } 1Cu^{2+} + 2e^- + Mo_6S_8 \rightleftarrows Cu_1Mo_6S_8. \quad (4)$$

At higher intercalation stages the structural changes are in formal agreement with the potential course of the coulometric titration of the molybdenum cluster sulfide. The continuous change in potential in region II of the potential/charge-transfer diagram (Fig. 4a, $\Delta G \neq$ const.) leading to the terminal compound $Cu_4Mo_6S_8$ is characterized by a continuous change in lattice parameters of a nonstoichiometric phase $Cu_xMo_6S_8$ with a phase width of $1 \leq x \leq 4$ (Fig. 4b; Eq. (4)). Figure 5b shows selected *in situ* X-ray diffractograms of the one phase region:

$$\text{One-phase region: } 3Cu^{2+} + 6e^- + Cu_1Mo_6S_8 \rightleftarrows Cu_4Mo_6S_8. \quad (5)$$

While in the potential/charge-transfer diagram the copper intercalation range $0 < x < 1$ appears to be characterized by two distinct two-phase regions, this section could definitely be identified as a single two-phase system with the coexisting phases Mo_6S_8 and $Cu_1Mo_6S_8$ by *in situ* X-ray studies. The hysteresis in electrochemical potential observed for forward and backward reaction can therefore be explained by the influence of kinetic factors. Similar phenomena have been reported by us for the systems Na/Mo_6S_8 and Cd/Mo_6S_8 (*20*), while no hysteresis is found in the case of Li/Mo_6S_8 (*21*),

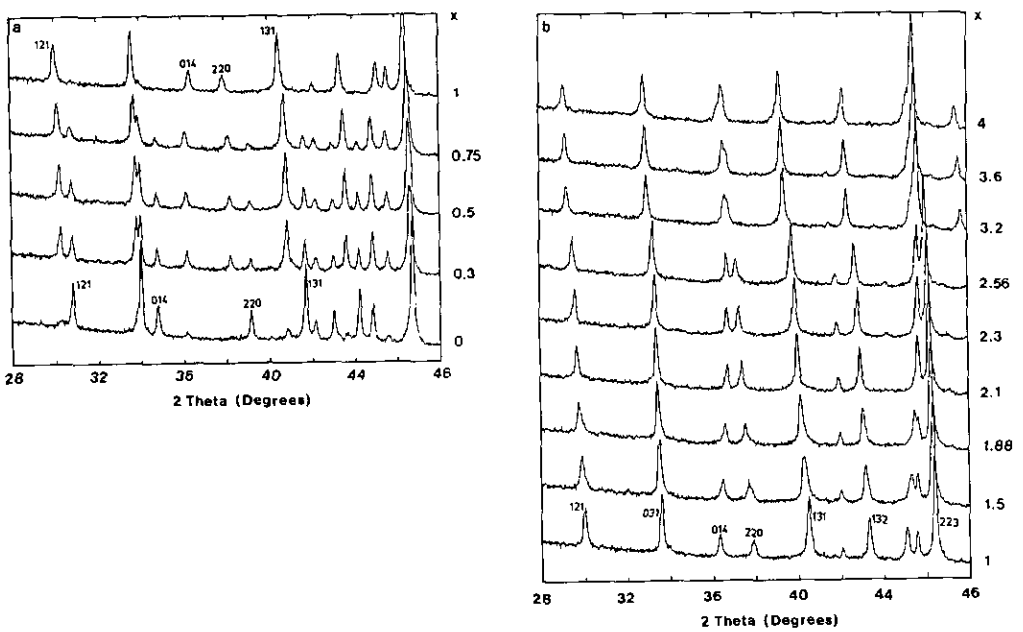

FIG. 5. X-ray powder diffraction patterns of Mo_6S_8 and ternary phases $Cu_xMo_6S_8$ recorded *in situ* during galvanostatic reduction of Mo_6S_8 (selected Bragg peaks labeled with hexagonal Miller indices): (a) Two-phase region $0 < x < 1$; (b) nonstoichiometric phase region $1 \leq x \leq 4$.

where the guest ion Li^+ has a hard-sphere ionic radius (60 pm) significantly below that of Na^+ (95 pm), Cu^+ (95 pm), and Cd^{2+} (97 pm).

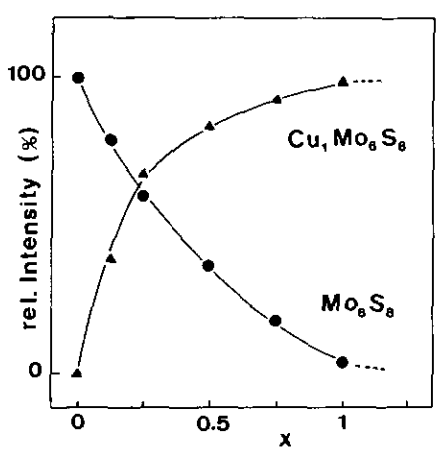

FIG. 6. Relative intensities (%) of the hexagonal 1 2 1 Bragg peaks of Mo_6S_8 and $Cu_1Mo_6S_8$ as a function of the copper content x. ●, Mo_6S_8; ▲, $Cu_1Mo_6S_8$.

Formation of $Cu_xMo_6S_8$ by Coulometric Titration of Mo_6S_8 in Aprotic Cu^+ Electrolyte

As already described, the aqueous cells revealed some specific problems, e.g., current density; it seemed necessary to carry out these experiments in aprotic electrolytes $Cu^0//Cu^{1+}$, $CH_3CN//Mo_6S_8$, for comparison reasons.

Figure 7 presents the potential/charge-transfer diagram obtained on galvanostatic cathodic reduction and anodic oxidation of Mo_6S_8 and $Cu_xMo_6S_8$, respectively, in Cu^ICl/CH_3CN at 300 K. A significant influence from the current density applied was not observed. It turned out that after an electrochemical charge transfer of $4e^-/Mo_6S_8$—using an aprotic Cu^{1+} electrolyte with $n(e^-/Mo_6S_8) = x(Cu/Mo_6S_8)$—the potential of copper deposition is reached; i.e., the intercalation reaction has arrived at its end point. Again, the maximum uptake of four

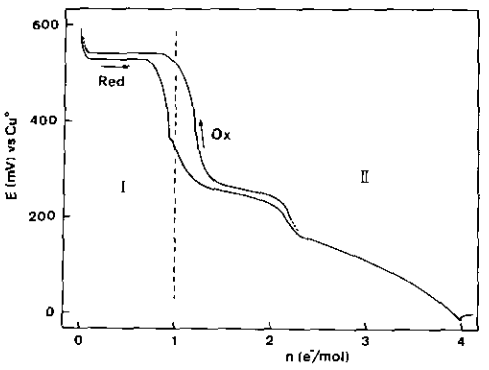

FIG. 7. Formation of $Cu_xMo_6S_8$ by galvanostatic cathodic reduction of Mo_6S_8 in aprotic Cu^I electrolyte at 300 K: Change in potential with the copper content x.

Cu^{1+} ions as predicted by the ionic structure model (*1*) and by the band structure calculations (*6*, *19*) is observed. Thermodynamic considerations suggest that the potential plateau in region I (Fig. 7) corresponds to a two-phase system, while region II with a continuous change in potential should represent a nonstoichiometric phase region. This is clearly verified by X-ray diffraction data with samples taken at different values of the electrochemical charge transfer: in region I the starting phase Mo_6S_8 coexists with $Cu_1Mo_6S_8$ as described by Eq. (6), while a nonstoichiometric phase $Cu_xMo_6S_8$ with a continuous change in lattice parameters is found in region II with a phase width of $1 \leq x \leq 4$ (Eq. (7)). The X-ray data are in good agreement with the values obtained by coulometric titration of Mo_6S_8 in aqueous Cu^{2+} electrolyte.

The galvanostatic anodic reoxidation of the fully intercalated ternary molybdenum cluster sulfide proceeds close to the equilibrium potentials in the range of $0 < n < 2.7$ ($n = e^-/Cu_4Mo_6S_8$). At lower copper contents a significant deviation of the potential curve of the coulometric reduction of Mo_6S_8 in aprotic Cu^{1+} electrolyte becomes obvious, contrary to the corresponding reaction in Cu^{2+}-containing aqueous electrolyte. While by galvanostatic reduction in $CuSO_4/H_2O$ significant hysteresis was observed in the range $0.5 < x < 1.5$, galvanostatic cycling of the cell $Cu^0//Cu^{1+}$, $CH_3CN//Cu_xMo_6S_8$ led to a much smaller width of the mentioned hysteresis of the $0.3e^-$/formula unit: $0.95 < x < 1.25$. Additional potentiostatic measurements characterized region I as a single two-phase system with ΔG = const. (-51.4 kJ · mole^{-1}; EMF = 0.53 V) within the limits $0 < x < 0.95$ (Eq. (6)).

$$\text{Two-phase region: } Cu^+ + e^- + Mo_6S_8 \rightleftarrows Cu_1Mo_6S_8 \quad (6)$$

$$\text{One-phase region: } 3Cu^+ + 3e^- + Cu_1Mo_6S_8 \rightleftarrows Cu_4Mo_6S_8 \quad (7)$$

The intercalation of small cations in Mo_6S_8 leads with deformation of the host matrix to the generation of 12 distorted tetrahedral sites around the unit cell origin (*1*, *2*). These positions can be distinguished as two concentric sets of six sites, i.e., pleated hexagonal rings with their planes perpendicular to the threefold lattice axis (Fig. 2). These sites are all interconnected and form infinite channels along the rhombohedral axis. They are essential for the transport properties of molybdenum cluster chalcogenides in terms of electronic/ionic conductivity at room temperature. Measurements of the chemical diffusion coefficient $\tilde{D}$ (300 K) by the galvanostatic intermittent titration technique (*16*) in aprotic Cu^{1+} electrolyte yielded values of 10^{-9} to 3×10^{-9} cm^2 · sec^{-1} for $Cu_1Mo_6S_8$ and $Cu_{1.5}Mo_6S_8$, respectively. For the ternary copper phases with $x = 2$ and 3 a chemical diffusion coefficient of about 1–2 orders of magnitude larger was observed with a slight increase in $\tilde{D}$ with increasing Cu content (Fig. 8). These data are not in agreement with the results of Dudley *et al.*(*15*), who observed no change in $\tilde{D}$ with the variation in Cu stoichiometry from $x = 1.5$ to $x = 3.37$ in $Cu_xMo_6S_8$. This increase of ionic mobility in the host lattice at room temperature may be due to the strong

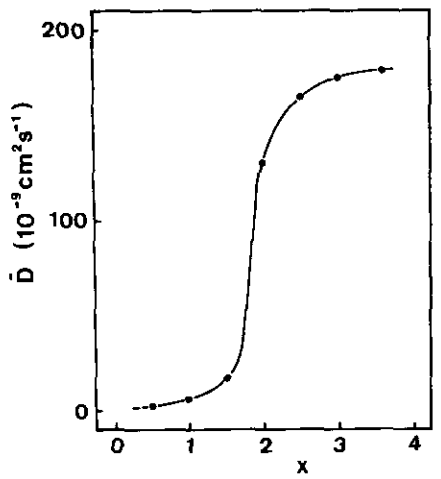

FIG. 8. Chemical diffusion coefficients $\tilde{D}$ of ternary phases $Cu_xMo_6S_8$ as a function of the integral copper content x (T = 300 K).

change in lattice distortion and unit cell volume (Table I). Yvon *et al.* (*22*) studied the site occupancy of Cu at site 1 and site 2 (Fig. 2) for thermal phases as a function of the copper content in $Cu_xMo_6S_8$. The authors report that in $Cu_xMo_6S_8$ only the first inner site Cu(1) is occupied at the lower limit of x (x = 1.8). Increasing x results in an increase in the occupancy of the second outer site Cu(2), leaving the population of the first site nearly unchanged. The increasing occupancy of Cu(2) sites leads to an enlarged origin S_1 distance while the origin S_2 distance remains unchanged. This implies that an increasing population of the outer Cu(2) sites leads to an enlarged system of intersecting vacant channels in the chalcogen atom network which allows an increase in the ionic mobility in the host lattice at higher intercalation rates. From a thermodynamic aspect, a change in slope of the potential of the electrochemical intercalation of copper at values of $x > 2.1$ appears; i.e., a change in the variation of the free energy ΔG with x must be noted (Figs. 4a and 7). At the mentioned region of the charge-transfer diagrams a minimum of the hexagonal c-axis is observed (Fig. 4b, Table I). The hexagonal c/a ratio decreases, however, over the whole range from Cu_1 to Cu_4 as expected.

A smaller c/a ratio and a larger rhombohedral angle indicate a deformation of the Mo_6S_8 host lattice; i.e., the origin S_8 pseudocube is compressed and distorted along the threefold axis. Meanwhile, the distortion of the original lattice is relatively large up to an integral copper content of $\approx$2.1 Cu/Mo_6S_8, and further intercalation of guest ions leads to significant lower structural changes (Table I). The region of the major lattice distortion correlates in fact with a significant change in transport behavior.

Structural Phase Transition of $Cu_{1.8}Mo_6S_8$ at Low Temperatures by in Situ X-Ray and ^{63}Cu NMR Studies

The first low-temperature studies performed by Flükiger *et al.* (*10*) revealed that rhombohedric copper Chevrel phases $Cu_xMo_6S_8$ undergo a triclinic phase transition. The transition temperature of $Cu_{1.8}Mo_6S_8$ was determined by specific heat (C) measurements as T = 269 K. Further indications for a sharp transition temperature of this phase at 269 K were given by a discontinuity in the slope of the temperature dependence of the electrical resistivity (*11*).

In order to verify the literature data, we made systematic temperature-dependent *in situ* X-ray measurements of $Cu_{1.8}Mo_6S_8$ prepared by thermal synthesis and compared the results to those from corresponding ^{63}Cu NMR experiments. The sample in the diffractometer was cooled by a flow of evaporating liquid nitrogen controlling the temperature with a precision of $\pm$0.5 K through electrical heat resistivity. Starting from 300 K the temperature of the solid was reduced in steps of 5 K with a cooling rate of 10 min $\cdot$ K^{-1} down to 90 K. The sample remained at constant temperature for 20 min in order to achieve thermal equilibrium. Figure 9 shows the diffraction patterns of $Cu_{1.8}Mo_6S_8$ in a 2Θ range between 36° and 48° at different

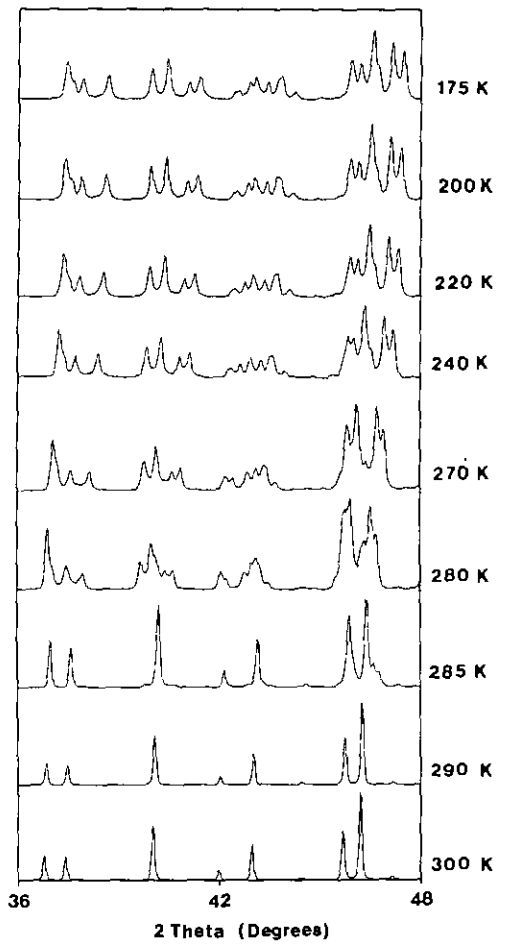

FIG. 9. Structural phase transition of $Cu_{1.8}Mo_6S_8$: Selected X-ray powder diffraction patterns in a temperature range between 300 and 175 K. (Intensities not proportional for reasons of a more distinct presentation.)

temperatures (300 K $\geq T \geq$ 175 K). Already at 285 K a splitting of the Bragg peaks is observed, indicating a first triclinic distortion of the $Cu_{1.8}Mo_6S_8$ lattice. By further lowering the temperature, the reduction in symmetry becomes more distinct and ends at 200 K, where the solid is completely converted to a triclinic phase. In fact, the structural phase transition does not occur at a definite temperature, as reported, but, assuming thermal equilibrium, in a wide temperature range between 285 and 200 K.

Reproducible results without any hysteresis were obtained by slowly reheating the sample under identical conditions. The lattice parameters of the rhombohedral (room temperature) and triclinic (low temperature) phase are listed in Table II. With the triclinic distortion of $Cu_{1.8}Mo_6S_8$ an order phenomenon, i.e., the formation of pairs of copper atoms (d_{Cu-Cu} = 258 pm (*23*), is observed, causing a slight contraction of the lattice volume (Table II) and a strong distortion of the cube shaped chalcogen cavity at the unit cell origin.

The subsequent distortion of $Cu_{1.8}Mo_6S_8$ was further investigated by corresponding temperature-dependent solid state ^{63}Cu NMR measurements (*17*). The spectrum at room temperature (T = 295 K) reveals one resonance signal (central line) with a linewidth (half-width at half intensity) of approx 36 kHz. The resonance frequency of ^{63}Cu nuclei amounts to 79.515 MHz. The chemical shift of $Cu_{1.8}Mo_6S_8$ (δ = −800 ppm vs $Cu^{I}Cl$) can be regarded as a downfield shift or paramagnetic shielding. The high resonance frequency in relation to copper metal with a chemical shift of δ = −2000 ppm $Cu_{1.8}Mo_6S_8$ implies partial covalent bonding.

Particular attention was given to the Cu NMR lineshape changes at lower temperatures in order to relate these to the X-ray data. By subsequent cooling of the thermal phase in steps of 5–10 K, a decrease in the signal intensity in connection with an intense line broadening was observed. At 200 K the resonance line almost fully disappeared from the noise level. If the temperature is lowered further, a new distinct resonance line is observed already at 190 K. Low-temperature spectra at 180 and 120 K reveal almost the same line intensity and line shift (signal width 80 kHz) as the original line at $T >$ 280 K. This increase of the signal width at low temperatures may be attributed

TABLE II

LATTICE PARAMETERS OF $Cu_{1.8}Mo_6S_8$ AT 300 K (RHOMBOHEDRAL PHASE) AND 200 K (TRICLINIC DISTORTED PHASE)

T(K)	a (pm)	b (pm)	c (pm)	α (°)	β (°)	γ (°)	$V \cdot 10^6$ (pm³)
300	650.2(3)			94.88(2)			271.1
200	643.9(4)	652.2(3)	651.3(3)	96.75(3)	93.49(2)	95.78(2)	269.5

to a strong magnetic interaction of the Cu nuclei due to the small nuclear distance in the low-temperature structure. The downfield shift of $Cu_{1.8}Mo_6S_8$ at 120 K (−600 ppm) is thus somewhat smaller than that at room temperature.

The loss of intensity of the Cu NMR signal in the temperature range between 295 and 200 K may be described by an order/disorder model. With decreasing temperature, only small isolated areas of the sample undergo triclinic distortion. Thus, some of the copper atoms experience a different structural environment leading to different field gradients. The strong differences in the electronic environment of the copper nuclei are explained by quadrupole interactions resulting in strongly broadened and less intense lines. The fact that only a small amount of copper atoms experience an equal structural and magnetic environment represents a state of strong structural and magnetic disorder. Finally, at temperatures near 200 K, rapid growth of the triclinic domains occurs, leading to uniform quadrupole interactions. Hence after termination of the structural phase transition below 200 K intense, although broadened, resonance signals appear again. The latter is in agreement with considerations about the above-mentioned formation of copper pairs (*23*): reduced Cu–Cu distances lead to stronger dipole–dipole interactions and thus to a distinct line broadening of the Cu resonance. Further investigations of thermally and electrochemically synthesized intercalation compounds of $Cu_xMo_6S_8$ are planned with the aim of analyzing the bonding relations of copper in the molybdenum cluster sulfide and of studying the ionic mobility of the ternary metal atoms in the three-dimensional solid matrix (*17*). Similar studies of the lithium intercalation systems Li/Mo_6S_8 and Li/Mo_6Se_8 have already exhibited that solid state NMR spectroscopy is a valuable tool for clearing up phase diagrams and for gathering valuable information about the bonding aspects and dynamics of the host species (*21*, *24*).

Superconducting Properties of Ternary Copper Phases $Cu_xMo_6S_8$

Investigations concerning the superconductivity of ternary molybdenum cluster chalcogenides $A_xMo_6X_8$ (A = metal atom, X = S, Se, Te) have been a major topic in many publications since their discovery in 1972 (*2*, *25*). The studies of the superconducting properties of the system Cu/Mo_6S_8 were performed on phases prepared by thermal synthesis but also on samples obtained via coulometric titration of Mo_6S_8 in aqueous Cu(II) electrolyte (*13*). Detailed investigations about the superconducting behavior of phases $Cu_xMo_6S_8$ synthesized electrochemically in aprotic Cu(I) electrolyte have not been performed so far. We also report here on the influence of air and humidity on the superconducting behavior of various copper Chevrel phases synthesized at high temperatures.

The quartz ampoules with the thermally

TABLE III

TEMPERATURE-DEPENDENT ac SUSCEPTIBILITY OF $Cu_xMo_6S_8$

x in $Cu_xMo_6S_8$	T_c onset (K)	Transition range (K)
(a) High-temperature phases synthesized at 1400 K		
1.8	10.1	3.5
2	10.8	2.7
3	5.3	1.0
3.66	<2.2	—
(b) Samples obtained by galvanostatic reduction of Mo_6S_8 in aprotic $CuCl/CH_3CN$ electrolyte		
1	5.3	3.7
2	10.4	2.5
3	6.0	3.0

synthesized $Cu_xMo_6S_8$ phases with $x = 1.8$, 2.0, 3.0, and 3.66 were opened in a glove box under inert gas atmosphere (Ar). While part of the material was immediately transferred into helium-filled (500 mbar) lithium borate glass capillaries and sealed in order to perform the temperature-dependent ac susceptibility measurements, the rest of the materials were exposed to air for 5 days before comparable amounts of them were encapsulated in capillary tubes. Both sample series were measured under identical experimental conditions. No differences in the induction signals, in height, in critical temperature (T_c midpoint), or in width of the transition were detectable between samples exposed to air and those stored under argon atmosphere. The T_c characteristics of the high-temperature copper Chevrel phases are listed in Table IIIa. For $Cu_{3.66}Mo_6S_8$ with its strongly distorted lattice ($\alpha_R = 95.56°$; $c/a = 1.05008$) close to the magic number of 24 electrons per cluster, where semiconducting behavior is expected (*1*), no decrease in the induction signal above 2.2 K (He-2) was observed. $Cu_2Mo_6S_8$ (NEC = 22) reveals, in agreement with theoretical band structure calculations (*6*) and earlier studies on samples obtained via galvanostatic copper intercalation at ambient temperature (*13*), the highest transition temperature with $T_c = 10.2$ K (midpoint).

Parallel susceptibility measurements were performed with ternary copper phases $Cu_xMo_6S_8$, synthesized by electrochemical techniques via potentiostatic ($x = 1$, 3, and 4) and galvanostatic ($x = 2$) modes in the cell $Cu^0//CuCl$, $CH_3CN//Mo_6S_8$ (in Ar atmosphere) at room temperature. Comparable quantities of the highly air-sensitive samples were sealed into capillaries under 500 mbar helium. Generally the intensities of the induction signals were approximately one order of magnitude smaller than those originating from the corresponding thermal samples. This phenomenon seems to be strongly connected with the size of the particles, which depends on the mode of preparation. The samples synthesized electrochemically at ambient temperature from Mo_6S_8 reveal a distinctly smaller particle size, leading to less distinct and broad phase transitions. The difference in morphology is understandable, if we consider that the binary host lattice Mo_6S_8 is prepared from thermally synthesized $Cu_2Mo_6S_8$ under chemical copper deintercalation (leaching technique). During this leaching process a reduction in crystallite size is observable even under an optical microscope. Beyond the reduction in height of the transition and the increase in the transition width, no further significant differences from the high-temperature phases were observed. The results from the temperature-dependant susceptibility measurements of samples prepared electrochemically in aprotic CuCl electrolyte are presented in Table IIIb.

Conclusion

Thermodynamically stable phases of $Cu_xMo_6S_8$ could be synthesized from the elements at high temperatures (1100°C) in the range $1.8 \leq x \leq 3.66$, which is in good agreement with experiments performed by Yvon *et al.* (*22*). We cannot confirm reports by Yamamoto *et al.* (*26*) on the formation of high-temperature phases of $Cu_xMo_6S_8$ with

$3.66 \leq x \leq 4$ (*2*, *11*). $Cu_4Mo_6S_8$ (number of electrons per cluster unit: NEC = 24), however, may easily be obtained via coulometric titration of the binary electron-deficient cluster chalcogenide Mo_6S_8 in aqueous or aprotic electrolyte at 300 K. The maximum charge transfer observed is thus in agreement with predictions from the ionic/covalent structure model and band structure calculations. The terminal product stoichiometry corresponds to the ionic formula $(Cu^+)_4[Mo_6S_8]^{4-}$ with four electrons, i.e., the maximum numbers taken up into the conduction band of the Mo_6S_8 matrix. Analysis of the structural changes with x for thermally and electrochemically prepared phases confirmed these results.

Warburg oxygen manometry turned out to be a new analytical tool with which to examine the copper content of ternary electronic/ionic conductors. Due to the kinetic stability of the Mo_6S_8 host lattice, the mobile guest ions Cu^I will be oxidized to Cu^{II} upon dissolution of the ternary compound in aqueous acid solutions under consumption of an equimolar amount of oxygen. This method has also been used for determination of the oxidation states of high-temperature superconductor oxides (*5*). The lower phase boundary of $x = 1.8$ in high-temperature $Cu_xMo_6S_8$ phases shifts down to $x = 1.0$ when copper is intercalated electrochemically. Nonstoichiometric phases of $Cu_xMo_6S_8$ with a homogeneity range of $1 \leq x \leq 4$ can be synthesized only at low temperatures. Solid state reactions of electronic conductors at room temperature thus offer a way of synthesizing new metastable phases which are not accessible by conventional thermal preparation. Since topotactic electron/proton transfer reactions via hydrogen bronzes play an essential role in many heterogeneous catalytic processes, intercalation compounds of $Cu_xMo_6S_8$ have been studied for the catalytic hydrogenation of acetylene and reduction of N_2. That activity has been interpreted in terms of the formation of $Cu_xH_yMo_6S_8$ intermediates and depends on the charge of the Mo_6 cluster (*5*). Investigation of the molybdenum cluster chalcogenides with their unusual properties in terms of the correlations of structure, bonding, physical properties, and chemical reactivity certainly remains an interesting field of solid state science.

Acknowledgment

The authors thank the Deutsche Forschungsgemeinschaft for support of this work.

References

1. K. YVON, *in* "Current Topics in Material Science" (E. Kaldis, Ed.), Vol II, p. 53, North Holland, Amsterdam (1979).
2. Ø. FISCHER AND M. B. MAPLE (EDS.), "Superconductivity in Ternary Compounds," Vols. I and II, Springer-Verlag, Berlin/Boston (1982).
3. R. SCHÖLLHORN, *Angew. Chem.* **92,** 1015 (1980); *Angew. Chem. Int. Ed. Engl.* **19,** 983 (1980).
4. R. SCHÖLLHORN, *in* "Inclusion Compounds" (J. L. Atwood, J. E. D. Davies, and D. D. MacNicol, Eds.), Vol. I, p. 249, Academic Press, London/New York (1984).
5. R. SCHÖLLHORN, *Angew. Chem.* **100,** 1446 (1988); *Solid State Ionics* **32/33,** 23 (1989).
6. T. HUGHBANKS AND R. HOFFMANN, *J. Am. Chem. Soc.* **105,** 1150 (1983).
7. R. CHEVREL, M. SERGENT, AND J. PRIGENT, *J. Solid State Chem.* **3,** 515 (1971).
8. R. CHEVREL, Thèse, Serie B, No. 186/112, Université de Rennes (1974).
9. A. C. LAWSON, *Mater. Res. Bull.* **7,** 773 (1972).
10. R. FLÜKIGER, A. JUNOD, R. BAILLIF, P. SPITZLI, A. TREYVAUD, A. PAOLI, H. DEVANTAY, AND J. MULLER, *Solid State Commun.* **23,** 699 (1977).
11. R. FLÜKIGER, R. BAILLIF, J. MULLER, AND K. YVON, *J. Less Common Metals* **72,** 193 (1980).
12. R. SCHÖLLHORN, M. KÜMPERS, AND J. O. BESENHARD, *Mater. Res. Bull.* **12,** 781 (1977).
13. R. SCHÖLLHORN AND M. KÜMPERS, *Mater. Res. Bull.* **14,** 1039 (1979).
14. J. MIZUSAKI, S. YITLAN, F. FUEKI, AND K. KITAZAWA, *Solid State Ionics* **11,** 293 (1984).
15. G. J. DUDLEY, K. Y. CHEUNG, AND B. C. H. STEELE, *J. Solid State Chem.* **32,** 259 (1980).
16. W. WEPPNER AND R. A. HUGGINS, *Annu. Rev. Mater. Sci.* **8,** 269 (1978).
17. W. NONTE, W. MÜLLER-WARMUTH, C. FISCHER, E. GOCKE, AND R. SCHÖLLHORN, in preparation.

18. J. C. W. Folmer and F. Jellinek, *J. Less Common Metals* **76,** 153 (1980).
19. O. K. Andersen, W. Klose, and H. Nohl, *Phys. Rev. B* **17,** 1209 (1978).
20. E. Gocke, W. Schramm, P. Dolscheid, and R. Schöllhorn, *J. Solid State Chem.* **70,** 71 (1987).
21. E. Gocke, R. Schöllhorn, G. Aselmann, and W. Müller-Warmuth, *Inorg. Chem.* **26,** 1805 (1987).
22. K. Yvon, A. Paoli, R. Flükiger, and R. Chevrel, *Acta Crystallogr. Sec. B* **33,** 3066 (1977).
23. K. Yvon, R. Chevrel, and M. Sergent, *Acta Crystallogr. Sec. B* **36,** 685 (1980).
24. G. Aselmann, W. Müller-Warmuth, E. Gocke, and R. Schöllhorn, *Z. Phys. Chem. NF* **151,** 103 (1987).
25. B. T. Matthias, M. Marezino, E. Corenzwit, A. S. Cooper, and H. E. Barz, *Science* **175,** 1465 (1972).
26. S. Yamamoto, K. Mitsui, M. Wakihara, and M. Taniguchi, *Mater. Res. Bull.* **18,** 1311 (1983).